

# Effect of Antenna Orientation and UAV Position on UAV Communications in 3D Space

N. Cameron Matson, Joseph Camp, Dinesh Rajan

Department of Electrical and Computer Engineering, Southern Methodist University, Dallas, TX, USA

Email: {cmatson, camp, and rajand}@smu.edu

**Abstract**—In this paper, we use the results of an in-field air-to-air (A2A) channel sounding experiment to build a model of the channel over the full range of azimuth and elevation angles. We use said model to analyze the effect antenna orientation and UAV relative position have on channel magnitude. First, we quantify the different ways in which the UAV body can alter the radiation pattern of a dipole antenna depending on whether the antenna is perpendicular or parallel to the body of the UAV. Then, we analyze the effect that change in the radiation pattern has on the cross-polarization discrimination (XPD). Finally, we calculate the overlapping index, a distance measure, between the distribution of channel magnitude in two symmetric regions of 3D space and observe that the two distributions are further apart when the receiver (Rx) is below the transmitter (Tx), suggesting an asymmetry in the way the Tx and Rx UAV body affect the channel.

**Index Terms**—A2A channel, unmanned aerial vehicles, wireless channel measurements, cross-polarization discrimination

## I. INTRODUCTION

Unmanned aerial vehicles (UAVs) are becoming increasingly prevalent in a number of application domains because of their high degree of mobility, low-cost, and ability to be deployed on-demand. Many research efforts involving UAVs have been focused on the design, simulation, and optimization of UAV deployment to in a variety of tasks such as emergency network coverage, search and rescue, and smart agriculture. A critical aspect of the design of these systems is an accurate understanding of the UAV wireless channel. There have been many studies of the UAV based wireless channel (see [1], [2] for a thorough overview of the space); however, many of the models developed in these studies are theoretical or are based on ray tracing simulations. While these are useful, it is fundamentally important that we also develop empirical models based on in-field measurements.

Of the limited number of empirical UAV channel models, the vast majority are based on air-to-ground (A2G) experiments. In many applications, however, it may be necessary for multiple UAVs to coordinate together, either to achieve a common goal or to avoid collisions while they carry out separate tasks. In these scenarios, it is necessary that the UAVs are able to establish and maintain reliable wireless connections amongst themselves over the air-to-air (A2A) channel. There are far fewer studies of the A2A channel. As with the study of A2G channels, many are either theoretical (e.g. [3]) or simulation based (e.g. [4]), though there have been a few empirical studies [5]–[8]. In [5], they explored

both pathloss and small-scale fading of the A2A channel at various horizontal and vertical distances. The authors of [6] performed several A2A experiments to develop a UAV-specific extension of the Rice Model. In our previous work [7], [8] we investigated the impact of varying the antenna placement, orientation, and polarization on both A2G and A2A channels.

In-air 3D communication between UAVs inherently depends on the strength of the channel between drones. For a given UAV-to-UAV distance, this A2A channel is a function of three variables: i) the alignment of the antenna radiation patterns, ii) the alignment of the antenna polarization, and iii) the degree to which the UAV body blocks (or reflects) the line-of-sight (LoS) path. Whereas our previous works dealt with a limited and discrete numbers of angles, in this work we expand upon the findings of those previous studies by presenting a full-3D model of the A2A channel and quantify the significant impact the relationship between antenna orientation and the Tx and Rx UAV bodies have on these variables. Specifically:

- We quantify the degree to which the UAV body alters the radiation pattern in the azimuth and elevation planes. The difference between antenna radiation patterns (isolated vs. drone-mounted) depends on the placement and orientation of the antenna relative to the UAV body. We find that placing the antenna in line with UAV body can reduce the channel magnitude by up to 12 dB vs. a perpendicularly mounted antenna at the same relative angle.
- The change in cross-polarization discrimination (XPD) is quantified as a function of the UAV body orientation with respect to the transmitting (Tx) antenna. We find that a Tx antenna mounted in line with the UAV body can cause the maximum XPD over all azimuth angles to be nearly twice ( $2\times$ ) that of a perpendicularly mounted antenna. In addition, when the Tx antenna is mounted in parallel with the UAV body, the standard deviation over all azimuth angles of the XPD is three-times greater than that of the perpendicularly mounted antenna.
- We show that there are asymmetries between the way that the Tx and Rx UAV body affects the channel. We do this by analyzing the empirical channel distribution between two otherwise symmetric hemispheres. This finding is surprising and has real implications for communication systems which may rely on channel reciprocity.

The remainder of the paper is constructed as follows: In Section II we introduce the measurement methodology and

describe the system model. The main analysis of the impact of the UAV-body-antenna-orientation relationship on the air-to-air channel is presented in Section III. We conclude in Section IV.

## II. METHODOLOGY AND SYSTEM MODEL

In this section we briefly introduce our UAV channel sounding platform, experimental methodology, and system model originally described in [9]. We also describe the coordinate system transformation used throughout this work.

### A. Experimental Setup

To measure the A2A channel in 3D space, we fly two UAVs simultaneously; one acting as a transmitter (Tx) and one as a receiver (Rx). Each UAV (DJI Matrice 100, shown in Fig. 1) carries an Ettus USRP E312 software-defined radio attached via a custom 3D-printed mount. The E312 has two independent RF chains that can function in Tx or Rx modes. We attach two antennas to Tx/Rx ports of the E312 at the front of the UAV. One antenna is mounted vertically (V) such that the length of the antenna is perpendicular to the body of the UAV and sticks out above the landing legs and propellers. The other antenna is attached horizontally (H), sticking out from the front of the UAV. Importantly, the horizontal antenna lies in the same plane as the UAV body and legs.

We use a spherical coordinate system, as shown in Fig. 1(a), to define the position of the Rx UAV. The underlying right-handed Cartesian coordinate system is oriented such that the positive x-, y-, and z-axes point East, North, and Up, respectively, with the Tx UAV at the origin. Locations in 3D space are described by an azimuth angle  $\phi^G \in [0, 360)$ , measured clockwise in the xy-plane from the negative x-axis, and an elevation angle  $\theta^G \in [-90, 90]$  defined as the angle above or below the xy-plane.

We collect the measurements over a series of experiments in a rural area near Taos, New Mexico to reduce the possibility of interference. In each experiment, the Tx UAV hovers at a fixed location at an altitude of 80 m and transmits constantly and simultaneously from both of its antennas using a carrier frequency of 2.484 GHz. The Rx UAV begins directly below the Tx and flies in a circle with a fixed radius of 20 m around the Tx by varying elevation angle. Both UAVs are oriented such that they face due North (i.e. the horizontal antenna points in the positive y direction.) During each flight, the Rx constantly receives on both of its antennas, but pauses for 10 seconds at points along the circle so that we can get stable channel measurements at specific angles. The entire campaign consists of 114 unique Rx hovering locations spanning the full range of both azimuth and elevation angle (thus covering 3D space) at a spacing of  $22.5^\circ$  in both directions.

### B. System Model

We model the discrete-time the  $2 \times 2$  A2A channel as:

$$\begin{bmatrix} y_V(n) \\ y_H(n) \end{bmatrix} = \begin{bmatrix} h_{VV} & h_{HV} \\ h_{HV} & h_{HH} \end{bmatrix} \begin{bmatrix} x_V(n) \\ x_H(n) \end{bmatrix} + \begin{bmatrix} z_V(n) \\ z_H(n) \end{bmatrix}$$

Where  $x_i(n)$ ,  $y_i(n)$ ,  $z_i(n)$  are the transmitted signal, received signal, and effective noise on antenna  $i \in \{V, H\}$  at time

instance  $n$ , and  $h_{ij}$  is the complex-valued SISO channel between Tx antenna  $i$  and Rx antenna  $j$ . We are thus able to measure four distinct channels: a co-polarized (VV, HH) and a cross-polarized (VH, HV) for each antenna orientation. We use continuous wave channel sounding, i.e. the signal transmitted from each Tx antenna is a complex sinusoid at a unique frequency which allows us to separate the signals at the receiver. We estimate the channel on blocks of data using a least squares estimation. Details on the experiment design, data processing, and estimation can be found in [9].

In this work, we primarily analyze the magnitude of the SISO channels,  $|h|^2$ , and quantify how it is affected by the orientation of the UAV body and relative position of the UAVs. We compare the measured channel magnitude to that of the theoretical channel based on the following two quantities:

1) *Antenna Radiation Pattern*: The magnitude of the channel is proportional to the pathloss<sup>1</sup>, which is a function of the product of the gains, or radiation patterns, of the Tx and Rx antennas,  $G_T$  and  $G_R$ . The theoretical radiation pattern of a vertical (oriented along the positive z-axis) dipole antenna is  $G_V(\phi, \theta) = \cos^2(\theta)$  [10]. Note that the pattern does not depend on the azimuth angle  $\phi$  and varies from its maximum value at  $\theta = 0^\circ$  to 0 at  $\theta = \pm 90^\circ$ . The magnitude of the channel between the co-polarized vertical antennas is thus proportional to  $G_V G_V$ , i.e.,  $|h_{VV}|^2 \propto G_V(\phi, \theta) G_V(\phi, \theta) = \cos^2(\theta)$ .

2) *Cross-Polarization Discrimination*: The XPD is the difference (in dB) in the received power between a co- and cross-polarized antenna pair. In a slight abuse of terminology, we define it here to be the difference in the channel magnitudes of the same. For example, for a vertically oriented Tx antenna, we have  $XPD_{V,dB} = 10 \log(|h_{VV}|^2) - 10 \log(|h_{VH}|^2)$ . In theory, the channel magnitude between a vertical Tx antenna and horizontal Rx antenna (or vice-versa) should be extremely low, resulting in low cross-polarized received power compared to the co-polarized, thus the XPD would be very high.

### C. Coordinate System Transform

We have already defined a global coordinate system which defines the position of the Rx UAV with respect to the Tx. Conveniently, this coordinate system is oriented such that the vertical antennas on the UAVs align with the z-axis. As described in the previous section, this makes the radiation pattern of this antenna a function of  $\theta$  only. However, if we were to describe the radiation pattern of the horizontal antenna, which lies along the y-axis in the global coordinate system, it would be a more complex function of both the azimuth and elevation angle.

Since the two antennas are fundamentally the same, aside from the orientation relative to the UAV, we want to analyze them using the same theoretical radiation pattern. To do this, we introduce the coordinate system shown in Fig. 1(c) which has the effect of rotating the UAVs such that the horizontal antenna is oriented along the *new* z-axis—i.e., it is vertically

<sup>1</sup>We consider only the large-scale free-space pathloss in this work as the experiment takes place in an open LoS environment at a sufficient altitude to avoid ground based multipath.

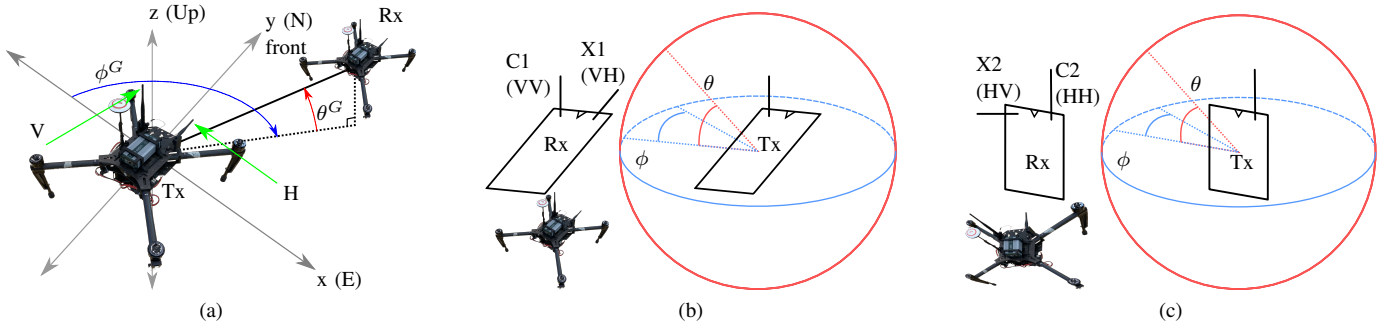


Fig. 1. (a) The global, UAV based coordinate system defining the relative position of Rx UAV to the Tx. (b) Orientation of the UAV body and the location of the co- and cross-polarized antennas in the Tx antenna based coordinate systems for UAV orientation 1 (the plane of the UAV body is perpendicular to the Tx antenna.) (c) The same for UAV orientation 2 (the long side of UAV body is parallel to the Tx antenna.) The notch represents the top, front of the UAV.

TABLE I  
CHANNEL NAMING CONVENTIONS

Global	Tx Based (Polarization, Antenna orientation to Tx Body)
VV	C1 (Co-pol, Perpendicular)
VH	X1 (X-pol, Perpendicular)
HH	C2 (Co-pol, Parallel)
HV	X2 (X-pol, Parallel)

oriented in the new coordinate system. This allows us to compare the effects of antenna orientation (or more specifically the angle between the UAV body and the antenna) for the vertical and horizontal against the same simple radiation pattern which only varies in  $\theta$ .

To emphasize that the Tx antenna is *always* vertical, in addition to referring to the channels by the antenna pair orientation with respect to the UAV (i.e., VV, VH, HV, or HH), we will occasionally describe the four channels as using the names C1, X1, C2, and X2, respectively. In this convention the first letter represents that the channel is either the co-polarized (C) or cross-polarized (X) and the second number represents whether the UAV bodies are perpendicular (1) or parallel (2) to the Tx antenna. We call this convention “Tx Based” because it signifies that angles are measured relative to the vertical orientation of the Tx antenna, regardless of its orientation in the global coordinate system.

For example, the channel between the two horizontal antennas (HH in the global coordinate system) is C2 because it is co-polarized and the Tx antenna is parallel to the UAV bodies. The equivalent naming conventions for the UAV based and Tx antenna based coordinate systems are summarized in Table I. Fig. 1(b) and (c) show the UAV and antenna configuration of C1, X1 and C2, X2 channels in their Tx antenna based coordinate systems, respectively.

### III. ANTENNA ORIENTATION AND POSITION EFFECTS

We now show the ways in which the relationship between the UAV bodies and antennas can affect the A2A channel. The original dataset consists of 114 unique locations spaced at  $22.5^\circ$  intervals over the azimuth and elevation angles in

the global coordinate system. This spacing is not preserved in the rotated system. In order to compare arbitrary angles in both systems coordinate systems, we perform a 3D scattered interpolation by first calculate a Delaunay Triangulation to generate a 2D surface in 3D space and then do natural-neighbor interpolation on each triangle at  $0.5^\circ$  spacing. This guarantees  $C^1$  continuity [11].

#### A. Impact of UAV-Antenna Orientation on Radiation Pattern

Fig. 2 shows 2D representations of the interpolated channel magnitude estimates  $|h|^2$  over all azimuth and elevation angles, along with a depiction of the UAV body and antenna configuration of both the Tx and Rx (as described in Section II-C) for that channel. The marked lines in (b) and (c) correspond to particular fixed values of azimuth and elevation angles which are plotted in polar coordinates in Fig. 3.

Figs. 2(a) and (b) show the effect of the coordinate transformation. The data is the same in both figures (they both show C1, i.e. HH), but (a) uses the global coordinate system while (b) uses the rotated, Tx based system. Fig. 2(c) shows the C1, i.e. VV, channel. The C1 channel behaves similarly to the theoretical radiation pattern of a vertical dipole antenna: it is strongest at small elevation angles, weak at large elevation angles, and shows little dependence on the azimuth angle. One might expect the C2 channel, in (b) to behave similarly since, theoretically, the radiation pattern is the same. Indeed, Fig. 2(b) shows that the channel is strongest at small values of  $\theta$  and weakest at large values; however, the channel is clearly not independent of the azimuth angle,  $\phi$ . At low elevation angles, the channel is significantly weaker at azimuth angles near  $0^\circ$  or  $180^\circ$ .

The reason for this decrease in the channel magnitude is that, at these azimuth angles, the UAV body blocks the line-of-sight path between the two antennas. This blockage only occurs in the parallel UAV body scenario because the antennas lie in the plane of the UAV body and legs, while the perpendicularly mounted antennas stick up above them.

Fig. 3 shows “slices” of both the C1 and C2 channel magnitudes as they vary over  $\phi$  (left) and  $\theta$  (right). The C1 channel varies much less with  $\phi$  than the C2 channel. The standard deviation of the C1 channel at  $\theta = 0^\circ$  over  $\phi$  is 2.7

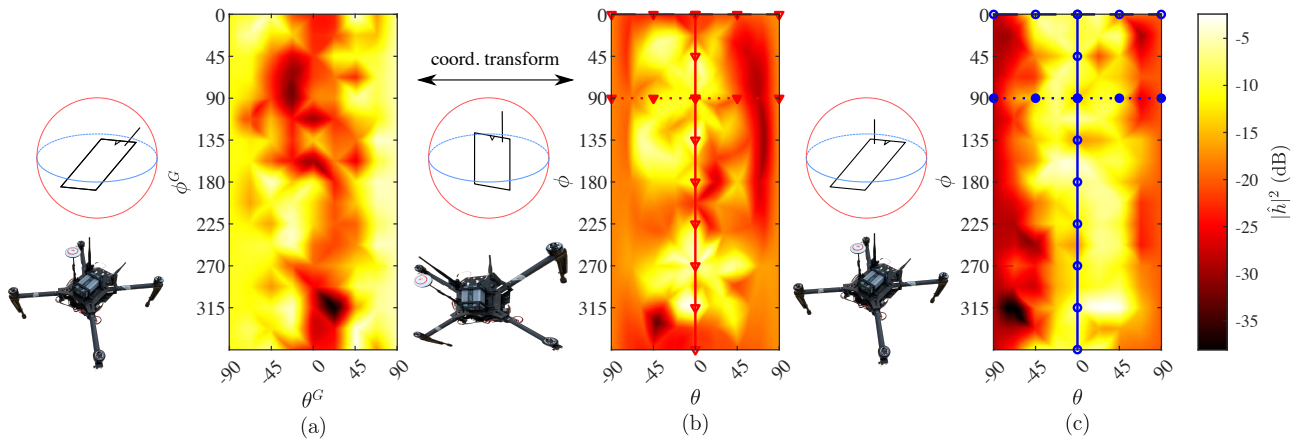


Fig. 2. Interpolated channel magnitude over 3D space of (a) the C2 (HH) channel in the global, UAV based coordinate system, (b) the same channel expressed in the Tx antenna based coordinate system, (c) the C1 (VV) channel. The differences between (b) and (c) are due to the UAV body blocking the link at azimuth angles around  $0^\circ$  and  $180^\circ$ . Marked lines as plotted in polar coordinates in Fig. 3

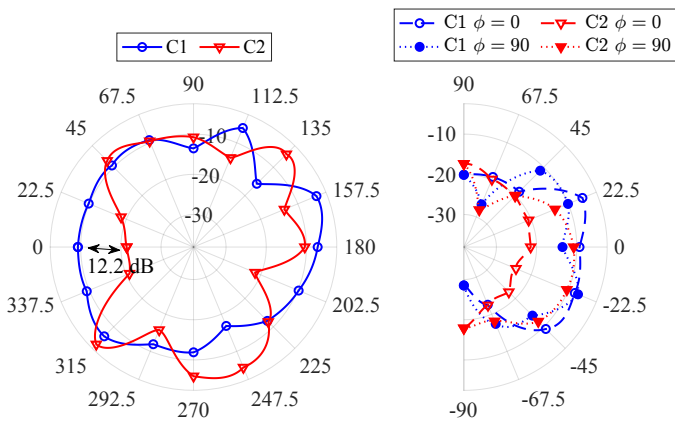


Fig. 3. Magnitude of the channel between the co-polarized antennas with different body orientations as described in Table I. (left) Variation over  $\phi$  with  $\theta = 0^\circ$ . (right) Variation over  $\theta$  with  $\phi \in \{0^\circ, 90^\circ\}$ .

dB, approximately half as much as that of the equivalent C2 channel at 5.2 dB. Additionally, the UAV body can reduce the magnitude of the C2 channel by up to 12 dB compared to the magnitude of the C1 channel at the same azimuth angle.

The orientation of the UAV body also effects the elevation angle dependence of the channel. Fig. 3(b) shows the channel magnitude vs. elevation angle of the C1 and C2 channels at two azimuth angles,  $\phi = 0^\circ$  and  $90^\circ$ . The path between the Tx and Rx for both C1 channels as well as the C2 channel at  $\phi = 90^\circ$  is mostly LoS, and the channel magnitude behaves similarly to the expected radiation pattern, i.e., strong at  $\theta = 0^\circ$  and decreasing towards  $\theta = \pm 90^\circ$ . The LoS path of the C2 channel at  $\phi = 0^\circ$ , however, is blocked by the UAV body regardless of the elevation angle. This channel is, therefore, generally weaker than the other three and does not vary as much with  $\theta$ . The standard deviation for each of these four scenarios is given in Table II.

### B. Impact of UAV-Antenna Orientation on XPD

In addition to affecting the radiation pattern, the UAV body produces local scattering of the signal which can cause polar-

TABLE II  
STD. DEV. OF CO-POLARIZED CHANNEL OVER ELEVATION ANGLE

	$\phi = 0$	$\phi = 90$
C1	6.5	5.7
C2	<b>1.8</b>	5.3

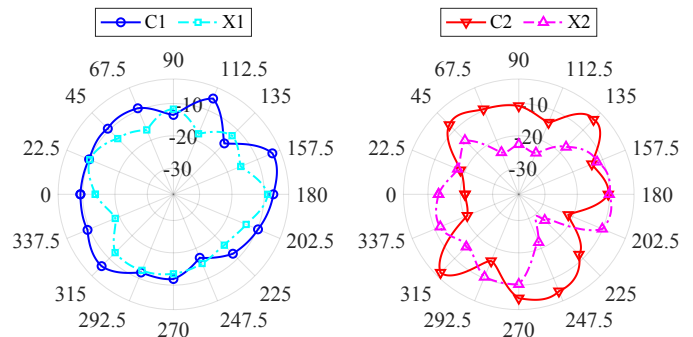


Fig. 4. Magnitude of the channels between co- and cross-polarized antennas over the  $\phi$  when (left) perpendicular to and (right) parallel with UAV body.

ization mixing, reducing the XPD [8]. Fig. 4 shows the channel magnitude of both the co- and cross-polarized channels over  $\phi$  at a  $\theta = 0^\circ$  in the Tx antenna based coordinate system for the two antenna/UAV body orientations: perpendicular (left) and parallel (right). The perpendicular case has been studied previously in [8], though the measurements were performed in an anechoic chamber with only the Rx antenna mounted on a UAV. Our in-field results here corroborate the finding that the UAV body reduces the XPD compared to that of an isolated pair of antennas. (The max XPD for the in-field experiments was 11.8 dB compared with 13 dB in the anechoic chamber measurements.) The right side of Fig 4, however, there is significant difference between the co- and cross-polarized channels, which results in a varying XPD at different azimuth angles.

Table III presents the statistics of the distribution of the XPD value over the set of all azimuth angles  $\{\phi\}$  at  $0^\circ$  elevation for the two different UAV body orientations. For example, the

TABLE III  
XPD STATISTICS OVER AZIMUTH ANGLE  $\phi$

	Max.	Min.	$\mu$	$\sigma$
XPD <sub>1</sub> = C1/X1	11.8	-3.4	4.0	2.9
XPD <sub>2</sub> = C2/X2	<b>21.2</b>	<b>-11.4</b>	<b>8.4</b>	<b>5.3</b>

“Max.” column is calculated as

$$\max_{\{\phi\}} \text{XPD}(\phi; \theta = 0).$$

The minimum, mean ( $\mu$ ), and standard deviation ( $\sigma$ ) are computed similarly with the exception that  $\mu$  and  $\sigma$  are computed using the absolute value of the XPD. Note that a negative XPD indicates that the cross-polarized link is stronger than the co-polarized.

The average and standard deviation of the XPD of perpendicular scenario, XPD<sub>2</sub>, are both roughly twice those of the parallel scenario. Additionally, the maximum and minimum XPD<sub>2</sub> are nearly two- and three-times those of XPD<sub>1</sub>, respectively. The takeaway is that while XPD<sub>1</sub> is relatively small and consistent over all azimuth angles, XPD<sub>2</sub> varies significantly between more extreme values.

The reason for this effect is two-fold and solely due to the orientation of the UAV body. On the one hand, when an antenna is mounted perpendicularly to the UAV body, the body causes enough scattering for polarization mixing to occur which reduces the XPD. On the other hand, when the antenna is mounted parallel to the UAV body, the body induces significant blockages that affect the co- and cross-polarized links differently at different azimuth angles.

### C. Impact of UAV Relative Position on Channel Distribution

In this section, we analyze how the relative position of the UAVs (rather than the orientation of the UAV body with respect to the Tx antenna) affects the distribution of the magnitude of the channel in an asymmetric way. We start by dividing the 3D space around the Tx UAV into two hemispheres, one in front of and one behind the Tx. Specifically, we define the following two sets of points

$$\mathcal{H}_f := \{(\phi, \theta) : 10^\circ < \phi < 170^\circ, |\theta| < 80^\circ\} \quad \text{and} \\ \mathcal{H}_b := \{(\phi, \theta) : 190^\circ < \phi < 350^\circ, |\theta| < 80^\circ\}$$

Where  $\mathcal{H}_f, \mathcal{H}_b$  are the set of points in 3D space that define the front and behind hemisphere, respectively. We limit the range of the azimuth and elevation angles to emphasize the difference between the two regions.

Then, we estimate the distribution of the channel magnitude over all azimuth angles in each hemisphere at each elevation angle as follows: Let  $H_\theta^s$  be a random variable that represents the channel magnitude  $|h|^2$  within hemisphere  $s \in \{\mathcal{H}_f, \mathcal{H}_b\}$  at elevation angle  $\theta$ . Then, we use kernel density estimation (KDE) to estimate the pdf:

$$\hat{f}_{H_\theta^s}(|h|^2) = \frac{1}{n\beta} \sum_{i=1}^n \Phi\left(\frac{|h|^2 - |h_i|^2}{\beta}\right)$$

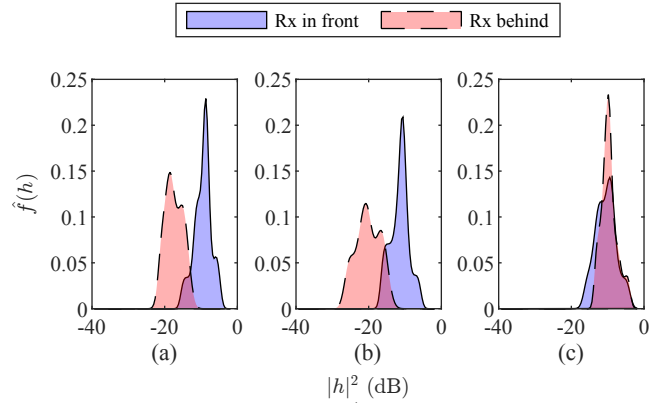


Fig. 5. Estimated density functions  $\hat{f}(|h|^2)$  of the VV channel magnitude  $|h|^2$  in the front and behind hemispheres at elevation angles  $\theta = \{-30.5^\circ, 43.5^\circ, 10^\circ\}$  for (a), (b), (c), respectively, estimated via Eq. 1. The overlap index in (a), (b), and (c) are  $\eta = 0.124, 0.411, \text{ and } 0.809$ , respectively, which in turn correspond to the minimum  $\eta$  when Rx is below, the minimum  $\eta$  when the Rx is above, and maximum  $\eta$  over all  $\theta$ .

where  $\hat{f}_{H_\theta^s}(|h|^2)$  is the estimate of the probability density in hemisphere  $s$  and elevation angle  $\theta$  at some channel magnitude  $|h|^2$ . We use the Gaussian kernel density function  $\Phi$  with the optimal (under the assumption that the true distribution is Gaussian) bandwidth parameter  $\beta$  [12]. The sum in (1) is taken over the  $n$  sample values of the channel magnitude  $|h_i|^2$ . There are  $n = 160/0.5 - 1 = 319$  sample values at each elevation angle because the samples span the  $160^\circ$  wide hemisphere at a  $0.5^\circ$  interval. The KDE is computed via the MATLAB function `ksdensity` [13]. Some example of estimated pdfs,  $\hat{f}(|h|^2)$  are shown in Fig. 5.

Fig. 6 shows the sample mean and standard deviation of channel magnitude at each elevation angle  $\theta$  for both hemispheres. The right y-axis shows the overlapping index [14]:

$$\eta = \int_{|h|^2} \min[\hat{f}_{H_\theta^f}(h), \hat{f}_{H_\theta^b}(h)] dh$$

which is a distance measure between two empirical distributions. When  $\eta(A, B) = 1$ , it implies that the two distributions  $A$  and  $B$  are identical, while  $\eta(A, B) = 0$  implies that  $f_A(x)f_B(x) = 0$  over the support  $x$  of  $A$  and  $B$ , i.e., the distributions are not the same.

Inspecting Fig. 6, we make the following three observations:

1) On average, the strongest channel does not occur at  $\theta = 0^\circ$  as one would expect based on the radiation pattern of a vertical dipole antenna. Instead, the strongest channel occurs around  $\theta = \pm 22.5^\circ$ . The sign of  $\theta$  depends on which hemisphere the Rx is in, i.e.,

$$\arg \max_{\theta} (|h(\theta)|^2) = -22.5^\circ$$

if the Rx is in front and  $+22.5^\circ$  if it is behind. This observation leads directly to:

2) One hemisphere (front or behind) is stronger than the other depending on whether the Rx is above or below (with the exception of a few degrees around 0). The mean channel magnitude in both hemispheres are approximately concave functions over most of the range of the elevation angle, and there is a single cross over point near  $\theta = 0^\circ$ .

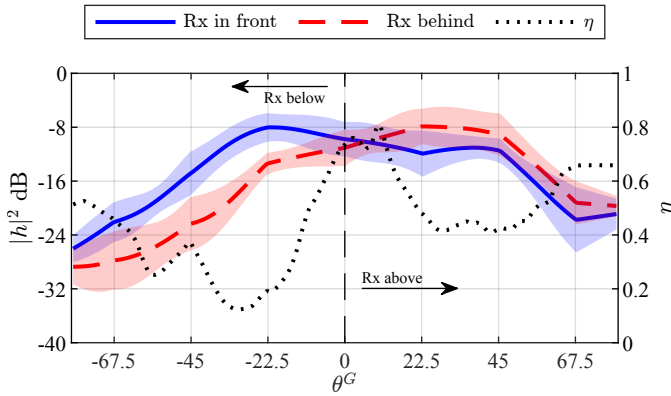


Fig. 6. Average channel magnitude ( $\pm\sigma$ ) of the VV channel over azimuth angles where the Rx UAV is in front of or behind the Tx UAV at different UAV based elevation angles  $\theta$ . The value of  $\eta$  is the percentage of overlap between the estimated “in front” and “behind” distributions.  $\eta = 1$  indicates that the pdf of the two distributions are equal.

3) There is more overlap between the estimated distributions at positive elevation angles than there is at negative angles. This is clear from the shaded regions which represent  $\pm\sigma$  around the average channel magnitude, and also corroborated by the value of  $\eta$ . When  $\theta < 0$ , i.e., when the Rx is below the Tx, the minimum value of  $\eta$  is 12%, which occurs at  $\theta = -30.5^\circ$  and the average is 35%. When the  $\theta > 0$  the minimum value of  $\eta$  is only 41% at  $\theta = 43.5^\circ$ , and the average is 56%. For reference, the maximum value of  $\eta$  is 81% and occurs at  $\theta = 10^\circ$ . Fig. 5 shows the estimated densities of the two hemispheres at these three elevation angles.

The underlying cause of each of these observations is the UAVs’ bodies and their relative position with respect to one another. One possible reason for the maximum channel to occur at non-zero elevation angles is that at  $\pm 22.5^\circ$  either the Tx ( $+\theta$ ) or Rx ( $-\theta$ ) UAV body is positioned in such a way that it can reflect the signal energy towards Rx antenna, forming a directional antenna.

This phenomena also explains why one hemisphere is exclusively better depending on the elevation angle. When the Rx is below the Tx: In the front hemisphere, the Rx body acts as a reflector and the Tx body is not in the LoS path; whereas in the behind hemisphere, the Rx body is not in the LoS path and the Tx body is *blocking* the LoS path. These UAV body relationships result in the “below/front” region being stronger than the “below/behind” region. A similar and reversed relationship exists between the hemispheres for positive elevation angles, where the Tx body can act as a helpful reflector, but the Rx body can only block the signal. The difference between the two “above” regions, however, is smaller than the two “below” as evidenced by the value of  $\eta$ .

The implication of these observations is that UAV bodies create an asymmetry in the behavior of the A2A channel. In other words, the reverse channel magnitude may be greater or weaker than that of the forward channel, despite the theoretical symmetries in the channel due to angular symmetries of the radiation pattern, because the UAV body affects the signal differently depending on whether it is the Tx or Rx.

## IV. CONCLUSION

In this work, we have analyzed the results of an air-to-air channel measurement study and isolated the effect of the configuration of the UAV bodies and the orientation of the antenna on the radiation pattern, cross-polarization discrimination, and distribution of the channel magnitude in 3D space. These effects have real implications for the communication link between UAVs, by effecting key parameters received signal strength, antenna diversity, and channel reciprocity. This analysis gives quantifiable justification for careful design of the UAV-antenna configuration for use in A2A systems. In the future, we will explore how the developed 3D model could be used to improve the accuracy of parameters (e.g., throughput and outage) in network simulations of A2A applications.

## REFERENCES

- [1] A. A. Khuwaja, Y. Chen, N. Zhao, M. Alouini, and P. Dobbins, “A Survey of Channel Modeling for UAV Communications,” *IEEE Communications Surveys Tutorials*, vol. 20, no. 4, pp. 2804–2821, 2018.
- [2] W. Khawaja, I. Guvenc, D. W. Matolak, U. Fiebig, and N. Schneckenburger, “A Survey of Air-to-Ground Propagation Channel Modeling for Unmanned Aerial Vehicles,” *IEEE Communications Surveys Tutorials*, vol. 21, no. 3, pp. 2361–2391, 2019.
- [3] Z. Ma, B. Ai, R. He, G. Wang, Y. Niu, and Z. Zhong, “A Wideband Non-Stationary Air-to-Air Channel Model for UAV Communications,” *IEEE Trans. Veh. Technol.*, vol. 69, no. 2, pp. 1214–1226, Feb. 2020.
- [4] L. Zhou, Z. Yang, G. Zhao, S. Zhou, and C.-X. Wang, “Propagation Characteristics of Air-to-Air Channels in Urban Environments,” in *2018 IEEE Global Communications Conference (GLOBECOM)*, Dec. 2018, pp. 1–6, iSSN: 2576-6813.
- [5] E. Yanmaz, R. Kuschig, and C. Bettstetter, “Achieving air-ground communications in 802.11 networks with three-dimensional aerial mobility,” in *2013 Proceedings IEEE INFOCOM*, Apr. 2013, pp. 120–124, iSSN: 0743-166X.
- [6] N. Goddemeier and C. Wietfeld, “Investigation of Air-to-Air Channel Characteristics and a UAV Specific Extension to the Rice Model,” in *2015 IEEE Globecom Workshops (GC Wkshps)*. San Diego, CA, USA: IEEE, Dec. 2015.
- [7] M. Badi, J. Wensowitch, D. Rajan, and J. Camp, “Experimental Evaluation of Antenna Polarization and Elevation Effects on Drone Communications,” in *Proceedings of the 22nd International ACM Conference on Modeling, Analysis and Simulation of Wireless and Mobile Systems*, ser. MSWIM ’19. New York, NY, USA: Association for Computing Machinery, Nov. 2019, pp. 211–220.
- [8] —, “Experimentally Analyzing Diverse Antenna Placements and Orientations for UAV Communications,” *IEEE Transactions on Vehicular Technology*, vol. 69, no. 12, pp. 14 989–15 004, Dec. 2020.
- [9] N. C. Matson, S. M. Hashir, S. Song, D. Rajan, and J. Camp, “Effect of Antenna Orientation on the Air-to-Air Channel in Arbitrary 3D Space,” in *2021 IEEE 22nd International Symposium on a World of Wireless, Mobile and Multimedia Networks (WoWMoM)*, Jun. 2021, pp. 298–303.
- [10] C. A. Balanis, *Antenna theory: analysis and design*, 4th ed. Hoboken: Wiley, 2016.
- [11] I. Amidror, “Scattered Data Interpolation Methods for Electronic Imaging Systems: A Survey,” 2002.
- [12] B. W. Silverman, *Density estimation for statistics and data analysis*, ser. Monographs on statistics and applied probability. Boca Raton: Chapman & Hall/CRC, 1998, no. 26.
- [13] MathWorks, “Kernel smoothing function estimate for univariate and bivariate data - MATLAB ksdensity.” [Online]. Available: <https://www.mathworks.com/help/stats/ksdensity.html>
- [14] T. E. Clemons and E. L. Bradley, “A nonparametric measure of the overlapping coefficient,” *Computational Statistics & Data Analysis*, vol. 34, no. 1, pp. 51–61, Jul. 2000.